Valence and C 1s Core-Level Photoelectron Spectra of Butan-2-ol

Emma E. Rennie,[†,‡] Ivan Powis,*[,§] Uwe Hergenhahn,[†,‡] Oliver Kugeler,[†,‡] Simon Marburger,[†,‡] and Tim M. Watson[§]

Fritz-Haber Institut der Max Planck Gesellschaft, Faradayweg 4-6, D-14195 Berlin, Germany, Max-Planck-Institute for Plasma Physics, Boltzmannstrasse 2, D-85748 Garching, Germany, and School of Chemistry, University of Nottingham, Nottingham NG7 2RD, U.K.

Received: July 29, 2002; In Final Form: October 8, 2002

Photoelectron spectra of the chiral molecule butan-2-ol spanning the full inner and outer valence regions and the C 1s core region are presented. The valence spectra are interpreted with the aid of outer valence Green's function calculations of the ionization energies. These were performed for each of nine possible conformational structures, each structure having been optimized by density functional calculations. The preferred gas-phase conformations can hence be identified. An assignment of the C 1s core spectrum is also achieved, and the vibrational structure observed on one band is fitted with two progressions. These are identified as C−H stretching and C−OH bending motions localized on the chiral −CHOH− carbanol carbon atom.

1. Introduction

When a chiral molecule is placed in an environment that is itself chiral, the ensuing enantiomer-specific interactions can be said to provide the basis for most methods of distinguishing chiral molecular enantiomers, for example, chromatographic separation with a chiral stationary phase or various spectroscopic effects seen in the molecular interaction with a circularly (or elliptically) polarized radiation field. Such interactions are also integral to many mechanisms postulated to explain the symmetry breaking leading to the observed homochirality of terrestrial biomolecules (such as the naturally occurring L-amino acids). In particular, enantioselective photochemical or photophysical processes occurring between prebiotic molecules and circularly polarized starlight[1,2] have often been invoked in such theories.[3−5]

A number of recent papers have focused upon the interactions between chiral molecular partners in van der Waals complexes,[6−11] which may also be interpreted to help develop a model and an understanding of chiral recognition phenomena in living systems. In many of these studies, butan-2-ol, one of the simpler optically active organic molecules, has been used as a prototype chiral molecular partner,[6,7,9,11] its relatively high volatility rendering it a particularly convenient practical choice for such supersonic molecular-beam studies. However, a complicating factor with this molecule is undoubtedly the existence of various rotational conformations, which has the potential to cloud interpretations depending on structural detail.

The possible conformations of butan-2-ol are displayed in Figure 1. A full mapping of the $\{\theta, \phi\}$ conformational space was obtained by Hagemann et al.[12] using molecular mechanics. This identified nine local minima. These alternative conformations are labeled using a notation introduced by Le Barbu et al.[9] and subsequently extended by King and Howard.[13] The conformation of the C_2−OH bond, represented as a dihedral angle ϕ, is denoted by a prefix that can be either "h-", "m-", or "e-" depending on whether the hydroxyl hydrogen is located anti to the hydrogen, methyl, or ethyl group, as shown in Figure 1. The C_3−C_2 bond conformation, θ, is then described by two additional letters. The first denotes the relation of the hydroxyl group and the methyl group attached to the C_3 carbon, either anti ("a") or gauche ("g"), and the second denotes the relation of the two methyl groups, which can again be either anti or gauche; thus the three C_3−C_2 bond conformations have the designations "-ag", "-gg", and "-ga". Relative energies of these nine conformers have since been calculated using either ab initio MP2 methods[9,13] or density functional methods[14] to allow for electron correlation, and the thermal population of all nine at room temperature can be predicted.

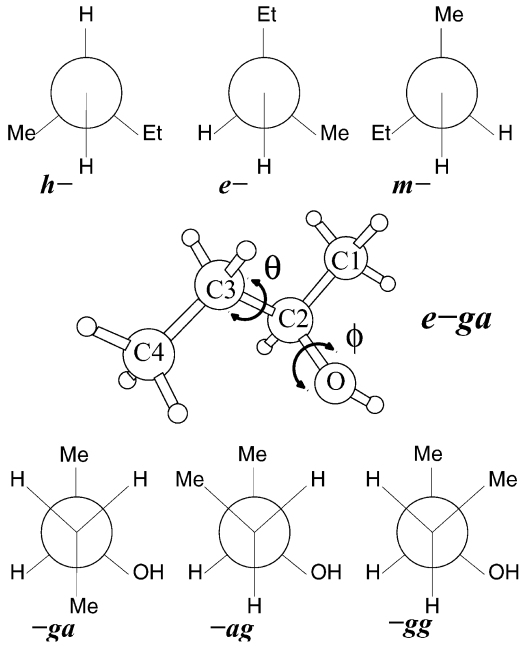

Figure 1. Conformational structures for *R*-(−)-butan-2-ol. The projections (top row) show the three minima for the dihedral angle ϕ, whereas those for the dihedral angle θ are shown on the bottom row.

* Corresponding author. E-mail: Ivan.Powis@Nottingham.ac.uk. Tel: +44-115-951-3476. Fax: +44-115-9513562.
† Fritz-Haber Institut der Max Planck Gesellschaft.
‡ Max-Planck-Institute for Plasma Physics.
§ University of Nottingham.

10.1021/jp026633c CCC: $22.00
Published on Web 11/27/2002

Confirmation of this prediction has been sought by spectroscopic experiments in both liquid and gas phases, with mixed outcomes. In CS_2 solution, the presence of all nine conformations was inferred from vibrational circular dichroism spectra,[14] but a less definitive result was obtained by Raman studies in the pure liquid,[12] where no conclusions regarding the C−OH conformations were reached. Similarly, microwave Fourier transform spectroscopy with a cooled molecular-beam source has produced only partial conclusions.[13] Just three distinct conformations were unambiguously identified, and whereas these clearly correspond to each of the three possible C_3-C_2 conformations -ag, -ga, and -gg, no equivalent certainty regarding the various C_2-OH conformations emerged because it was unclear whether certain possibilities were absent or were, for other reasons, simply indistinguishable. However, an additional complication in this latter experiment was the use of a supersonic molecular beam so that true thermal equilibrium in the sample was almost certainly not achieved. Consequently, there is a need for further gas-phase investigations to better clarify the population and behavior of the alternative conformers under solvent-free conditions and at true thermal equilibrium.

The photoionization of gas-phase butan-2-ol has received very little attention to date. To the best of our knowledge, the only published photoelectron spectrum offering any degree of detail is the He I valence spectrum published by Peel and Willett,[15] although a second, low-resolution "thumbnail" overview spectrum has also appeared as part of a wider-ranging study of various alcohols, mercaptans, and amines.[16] In addition, numerical values for the first (vertical) ionization energy and the O 1s core binding energy have been reported without accompanying spectra.[17] Finally, the unimolecular ion decay dynamics have been examined in a threshold photoelectron−photoion coincidence study and a threshold (adiabatic) ionization potential has been determined.[18]

Photoionization by circularly polarized vuv radiation provides a relatively novel form of chirally discriminating photon−molecule interaction and has recently been examined in the literature.[19−21] This interaction is manifested as an unequal emission of photoelectrons in the forward and backward directions (relative to the photon propagation direction), depending on the relative handedness of the light and the enantiomer. Such circular dichroism in the angular distribution of electrons (CDAD) from randomly oriented chiral molecules arises purely from electric dipole interaction and as such is predicted to be a more pronounced effect than normal circular dichroism (CD) in the total absorption cross section.[19,20] The precise detail of the predicted electron angular distribution is, however, structurally sensitive, as may be anticipated by recognizing that the phenomenon is essentially a diffraction of the polarized photoelectron by the chiral molecular ion. Any detailed theoretical interpretation of CDAD results will therefore require, at least at the outset, a sound understanding of the molecular conformation(s) adopted in the conditions pertaining to an experiment.

Studies of the amino acid alanine illustrate this point, since numerical calculations of the detailed orbital, angular, and photon energy dependence of the photoionization are quite distinct for each of the three low-lying conformations considered.[20] Yet whereas these conformers could be expected, from molecular orbital calculations,[22,23] to coexist with approximately equal population in a sample at thermal equilibrium, consistency between experimental ionization energies established from the gas-phase photoelectron spectrum[24] and those calculated was obtained for just one of the alternative conformations. The inference, that only one conformation is in fact important, is corroborated by other, more direct experimental evidence. Rotational spectra recorded in a free-expansion jet identify only two conformers, with at least an 8-fold dominance by one over the other.[25] Similarly, gas-phase electron diffraction results[26] were explained by reference to the same dominant single conformation.

From the foregoing, butan-2-ol might be considered an experimentally convenient choice for the study of chiral molecule CDAD subject to (i) clarification of the role of the alternative conformations in a gas-phase sample and (ii) extension of the baseline knowledge covering the ionization of this molecule. These then are the objectives for the present study of the photoelectron spectroscopy of butan-2-ol. Experimental spectra covering the inner and outer valence region up to 40 eV were obtained using synchrotron radiation and are compared with a comprehensive computational study of all nine suggested conformations. This is complemented by a measurement of the ∼357 eV C 1s core ionization spectrum of this molecule.

2. Experimental Details and Data Analysis

Spectra were recorded on the UE56/2-PGM[27] undulator beamline at the BESSY II synchrotron radiation source in Berlin with a Scienta SES-200 hemispherical electron spectrometer[28] mounted in a large spherical chamber. The beamline provides control of the light polarization, and both pure linear and circular polarizations can be selected in an energy range extending from about 60 to 1400 eV.[27] All of the spectra were measured using a 400 l/mm grating.

Two slightly different instrumental configurations were employed for different light-polarization states. In the first (**I**), the electron analyzer was mounted outside of the dipole plane under a forward scattering angle of 54.7° with respect to the beam direction. This was employed for both valence and core-level measurements with circularly polarized light. In the valence region, further measurements were made with linearly polarized light. The analyzer was now placed in the dipole plane at an angle of 54.7° with respect to the electric vector (**II**). In both cases, therefore, the electron acceptance is at the magic angle for the second Legendre polynomial term in the electron angular-distribution expression, and thus the recordings made in this work with either linear or circular polarization should be insensitive to the photoelectron asymmetry parameter β. Furthermore, we can anticipate that for the high electron kinetic energies included in this study any chiral effects in the angular distribution will be minimal;[19,20] consequently, the spectra presented here should be effectively independent of the chosen polarization.

Liquid butan-2-ol samples were held in a stainless steel reservoir. After several freeze−pump−thaw cycles, sample vapor from this reservoir was admitted via a leak valve to a gas cell inside the main vacuum chamber where photoionization occurred. The gas cell incorporated apertures for the synchrotron radiation and photoelectrons as well as a photoelectron dump to prevent backscattered electrons from entering the analyzer. The pressure in the main chamber was maintained at $\sim 5 \times 10^{-6}$ mbar ($\sim 1 \times 10^{-5}$ mbar for the core ionization measurements). All spectra were recorded by repetitive scanning to minimize the effects of any small temporal drifts and the decline in synchrotron beam intensity.

Valence spectra of racemic and enantiomeric *S*-(+)-butan-2-ol samples were recorded using linearly polarized light with an incident photon energy of 90 eV, (configuration **II**). An analyzer pass energy of 20 eV was employed, and spectrometer and monochromator slit settings were chosen to produce an

overall electron energy resolution of 55−60 meV, measured as the fwhm of the Ar 3p line. Spectrometer energy calibration was performed by recording Ar 3p, 3s, and correlation satellite lines[29] immediately before and after the experiments. We believe any residual error in our quoted values to be better than ±0.1 eV The adiabatic ionization energy estimated from these spectra is within better than 0.1 eV of the NIST[30] evaluated value of 9.88 ± 0.03 eV, and the first vertical ionization energy agrees equally well with the earlier quoted value of 10.35 eV.[15]

Further valence measurements were made with circularly polarized light (in configuration **I**) using *S*-(+) and *R*-(−) enantiomers at a photon energy of 80.33 eV. In these instances, the gas cell was also replaced by a sample inlet needle. Different slit settings were also used, yielding an estimated resolution of ∼100 meV. The spectrometer was calibrated using the xenon 5s main and satellite photoelectron lines[31] measured with an incident photon energy of 111 eV. However, a monochromator software problem, which was not identified at the time, has resulted in a relatively large uncertainty in the absolute energy scale. We therefore have also employed a secondary calibration against the above linearly polarized spectra.

High-resolution core-level spectra of *R*-(−)- and *S*-(+)-butan-2-ol C 1s were measured with an incident photon energy of 357.9 eV (circular polarizations, configuration **I**). The incident photon energy was calibrated using the argon 2p photoelectron lines, and the spectrometer was calibrated by checking the kinetic energy of the Xe NOO Auger lines.[32] The spectra were obtained with a beamline exit-slit setting of ∼60 μm, an electron analyzer slit width of 0.2 mm, and a pass energy of 40 eV, corresponding to an overall estimated resolution of 90 meV.

Successive C 1s spectra were summed and then analyzed with a least-squares fit that assumed two vibrational progressions, $\nu_{(1,2)}$, with Franck−Condon factors following a product of two Poisson distributions; they also allowed for the effect of postcollision interaction.[33] Each progression was modeled by the use of the linear coupling harmonic-oscillator approximation. Only the intensity $I(\upsilon' = 0)$ of the 0−0 transition is then treated as a free parameter, and the intensity of the other vibrationally excited states in the series follows the expression $I(\upsilon') = I(\text{total})\text{-}(S^{\upsilon'}/\upsilon'!)\exp(-S)$. From this one obtains $I(0) = I(\text{total})\exp(-S)$ and $I(\upsilon') = I(0)(S^{\upsilon'}/\upsilon'!)$. The dimensionless quantity S in these expressions is usually referred to as coupling constant. From the harmonic approximation it also follows that the states in each progression are equidistant in energy.

3. Computational Details

Calculations were performed using the Gaussian 98 and GAMESS (U.K.) packages. To calculate ionization energies (IEs), a full set of geometrical parameters is required for each conformational structure (Figure 1) so that, guided by the conformational map of Hagemann et al.,[12] optimized geometries were obtained by a density functional theory (DFT) calculation performed using a B3LYP functional[34,35] and the 6-31G** basis set. The default (75, 302) "fine" grid in Gaussian 98 was used for numerical integral evaluation. Results of these optimizations are presented in Table 1.

The relative energetic ordering of these structures is the same as for a similar recent DFT calculation using the 6-31G* basis[14] but differs somewhat from that of an alternative MP2/6-31G** study.[13] Relative energies expressed as differences from the lowest-energy conformation in this latter study have been included in Table 1. Although the DFT calculations order the lowest three conformers as h-ga < e-ga < m-ga, the MP2 calculation gives the ordering as e-ga < h-ga < m-ga. Given the small differences involved, it is not too surprising to find an element of disagreement between methods. Other differences between the ordering of the various -ag and -gg conformations in the DFT and MP2 calculations are noted, but certainly the DFT calculations confirm the stability of the carbon skeleton conformations in the order -ga < -ag < -gg estimated in earlier studies.[9,36]

TABLE 1: B3LYP/6-31G Optimized Geometries and Energies for the Nine Conformational Structures of Butan-2-ol Defined in Figure 1**

conformation	absolute energy (au)	ΔE (cm^{-1})	ψ^a	ϕ^b	population[c] %	ΔE (cm^{-1})[d]
h-ga	−233.685586	0.0	177.57	−63.97	30.16	13
e-ga	−233.685250	73.8	177.23	176.56	20.85	0
m-ga	−233.685005	127.7	180.67	65.36	15.93	88
h-ag	−233.684337	274.3	64.30	−63.97	7.65	303
m-ag	−233.684278	287.3	65.06	56.05	7.17	239
e-ag	−233.684133	319.0	66.02	180.77	6.12	290
m-gg	−233.683989	350.7	−61.59	57.70	5.22	217
e-gg	−233.683688	416.6	−61.43	181.48	3.76	285
h-gg	−233.683525	452.5	−64.62	−71.75	3.14	435

[a] Dihedral angle $\angle C_4-C_3-C_2-C_1$. [b] Dihedral angle $\angle C_3-C_2-O-H$. [c] Boltzmann population $T = 300$ K. [d] MP2/6-31G** energies relative to the e-ga ground state reported in ref 13.

TABLE 2: B3LYP/6-31G Optimized Geometries and Energies for the -ga Conformations, as in Table 1, but Using an Ultrafine Integration Grid**

conformation	absolute energy (au)	ΔE (cm^{-1})	ψ	ϕ
h-ga	−233.685595	0.0	177.57	−64.46
e-ga	−233.685257	74.2	177.23	176.57
m-ga	−233.685018	126.6	180.36	65.41

A potential limitation to the accuracy of grid-based DFT methods is the size of the grid used for numerical integration. To check this, the geometry of the three -ga conformers (judged the most important) were reoptimized using Gaussian 98's "ultrafine" (99, 590) grid. Results are shown in Table 2. The differences are minor, the biggest change (<0.5°) being seen in the dihedral angle ϕ. It was therefore concluded that the default grid provides acceptable performance.

All subsequent calculations were performed at the B3LYP/6-31G** optimized geometries of Table 1. Estimates of the vertical ionization energies, I_{vert}, of each conformer were calculated by the outer valence Green's function (OVGF) method[37,38] using a cc-pVDZ basis set. This includes a treatment of electron correlation in the framework of a one-particle hole model for the ionization. The results for 15 of the 16 valence orbitals are collected in Table 3. For each conformer, the calculated pole strengths in the OVGF calculation decreased from ∼0.92 to ∼0.84 in going from the 1st, outermost orbital to the 15th, but for the inner valence 16th orbital (eigenvalues ≈ −33 eV), the one-particle hole description unsurprisingly failed completely, and a full account of electron correlation is required.

A limited further investigation of the likely importance of electron correlation effects was undertaken for the representative h-ga conformer by performing two-particle hole Tamm−Dancoff (2ph−TDA) calculations[39] using the GAMESS (U.K.) package. The interaction space was restricted to the valence orbitals and the first four virtual levels. The results remained essentially diagonal up to IE ≈ 16 eV, beyond which mixing with neighboring excitations giving off-diagonal contributions gradually became apparent. Although too restricted a calculation to provide quantitative results, this suggest that a gradual failing of the independent electron model sets in above 16 eV.

TABLE 3: Vertical Ionization Energies (eV) for Butan-2-ol[a]

experimental I_{vert}		calculated I_{vert} energies									
this work	ref 15	h-ga	e-ga	m-ga	h-ag	m-ag	e-ag	m-gg	e-gg	h-gg	orbital no.
10.33	10.35	10.21	10.33	10.21	10.16	10.21	10.35	10.24	10.31	10.17	21
11.49	11.55	11.45	11.25	11.45	11.47	11.46	11.28	11.37	11.28	11.39	20
12.18	12.29	12.24	12.16	12.35	12.18	12.26	12.11	12.16	12.07	12.28	19
		12.25	12.28	12.66	12.39	12.37	12.51	12.42	12.18	12.37	18
12.68	12.75/	13.09	12.73	12.72	13.06	13.10	12.78	13.19	12.88	13.07	17
(13.1)	12.99										
13.48	13.47	13.24	13.41	13.50	13.69	13.49	13.40	13.29	13.63	13.56	16
	14.16	14.30	14.18	13.72	13.87	13.74	13.73	13.70	13.75	13.83	15
		14.66	14.67	14.68	14.85	14.48	14.59	14.00	14.55	15.01	14
14.95	14.93	15.11	14.91	14.95	15.11	14.90	15.32	15.52	15.09	15.20	13
(15.65)	15.94/	16.14	15.26	15.72	15.92	15.81	15.74	15.78	15.69	15.83	12
16.07	16.37										
(16.65)	17.24	16.04	17.39	17.41	16.42	17.32	17.05	17.00	17.19	16.49	11
17.26											
19.22		19.91	19.38	19.44	19.76	19.41	19.22	19.27	19.10	19.49	10
20.97		21.23	21.23	21.23	21.52	21.40	21.58	21.45	21.56	21.68	9
23.12		23.85	23.77	23.95	23.73	23.75	23.68	23.74	23.66	23.81	8
24.79		25.39	25.37	25.43	25.47	25.48	25.46	25.39	25.37	25.41	7
31.92											

[a] The absolute accuracy of experimental values is generally to within <0.1 eV, with minor peaks identified being shown in parentheses (see text). OVGF/cc-pVDZ calculated values are obtained for each conformer at the optimized B3LYP/6-31G** geometry and are ordered by the orbital eigenvalue rather than the IE

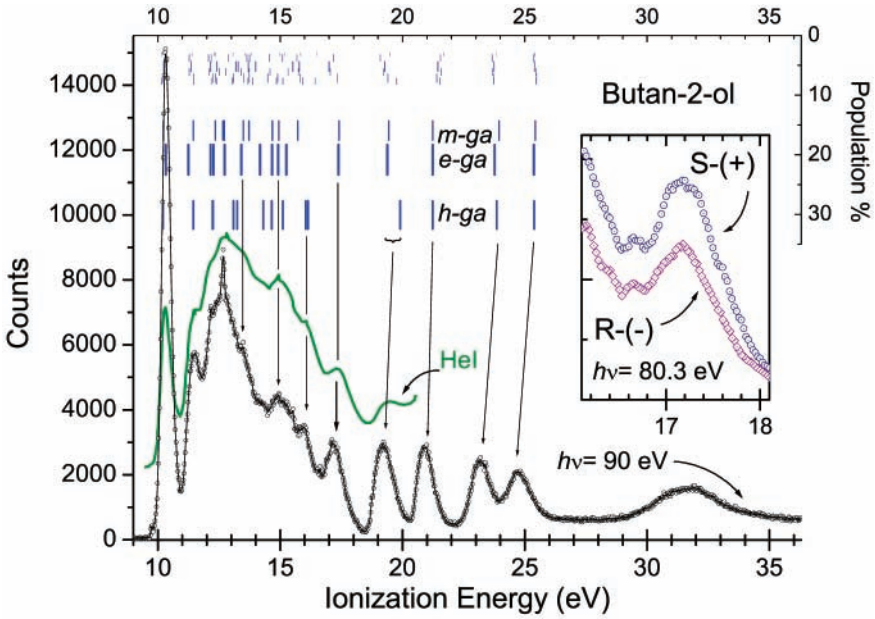

Figure 2. Full-range valence photoelectron spectrum of butan-2-ol. The main scan was recorded with a racemic sample using linearly polarized light ($h\nu = 90$ eV). For comparison, the He I spectrum, drawn according to ref 15, is arbitrarily scaled and over plotted. Calculated OVGF vertical ionization energies (Table 3) are also marked, indicating the estimated 300 K Boltzmann population (Table 1) on the right-hand scale. Alternative estimates of the relative populations, deduced from MP2/6-31G* energies,[13] are indicated by the relative size of the marker. The inset carries details from analogous scans made with enantiomeric *S*-(+)- and *R*-(−)-butan-2-ol using circular polarization ($h\nu = 80.3$ eV) to show the reproducibility of even the minor features.

4. Experimental Results and Discussion

4.1. Valence Spectra. An overview of the full experimental valence-region spectrum is shown in Figure 2. The data in fact extend from 5 to 40 eV, but no additional structures are found outside the central region included in the Figure. These spectra extend to higher energies the earlier He I spectrum of Peel and Willett,[15] which is also included in the Figure. Comparison of the calculated ionization energies (Table 3) with the present experiments is best accomplished visually, so for each conformer these data are marked in the upper panel of Figure 2 against their estimated room-temperature population (Table 1). Alternative population estimates based upon the MP2/6-31G* calculated energies[13] are simultaneously indicated by weighting the relative size of the plot markers. Whichever population estimate is preferred, it is clear that the three -ga conformations dominate.

For discussion purposes, it is convenient to divide the spectrum into two regions above and below 18 eV corresponding, loosely, to what may be considered the inner and outer valence regions. In the former region, the OVGF results for all of the various conformers clearly cluster into four bands, which may be correlated with the four distinct experimental bands in the 18−26 eV region as shown. The OVGF results seem systematically to overestimate the experimental IEs in this region, a tendency noted in an analogous study of alanine.[40] There is expected to be a gradual degradation of the validity of the OVGF one-particle hole model across this region as electron correlation increases for deeper-lying orbitals. Indeed, the OVGF

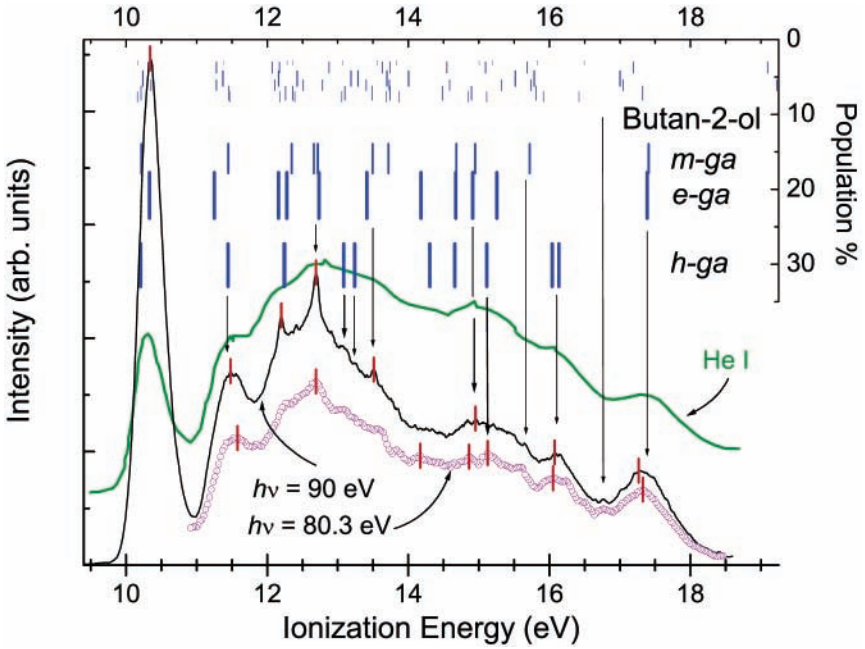

Figure 3. Expanded high-resolution detail of the outer valence region. The main curve is an oversampled (0.01 eV) scan of racemic butan-2-ol using linear polarization ($h\nu = 90$ eV). Located peak positions are marked on the trace. A lower-resolution scan of the same region made with the R-(−) enantiomer using circular polarization ($h\nu = 80.3$ eV) and arbitrarily scaled is added for comparison, as is the He I spectrum[15]. Other details are the same as in Figure 2

method fails to give a meaningful result for the innermost valence orbital (eigenvalue approximately −33 eV). It is nevertheless tempting to associate this orbital with the last broad band seen around 32 eV, but our limited 2ph-TDA calculations suggest that rather, as a consequence of electron correlation, this peak results from a number of weak, broad overlapping transitions to mixed ionic configurations.

At the other extreme, in the outer valence region, a more complex correlation between theory and experiment is obtained. A more detailed examination of this region, below 18 eV, is contained in Figure 3. The main trace here has been oversampled with 0.01-eV step intervals to improve its S/N and general definition. Experimental peak positions were located by an automated search routine applied to our spectra and are listed in Table 3 and marked on the spectrum in Figure 3. A number of other structures, which did not meet the strict statistical tests of the peak-picking routine but are nevertheless seen by close visual inspection, are also listed in parentheses in Table 3. These minor features are quite reproducible. For example, the small feature seen in the valley at 16.65 eV is also evident in the second, lower-resolution spectrum (*R*-(−)-butan-2-ol, $h\nu = 80.3$-eV photons) presented in Figure 3 and is also present in the main spectrum in Figure 2 (though harder to discern because of the scale); it can be most clearly seen in the two expanded enantiomer spectra shown in the inset of the latter Figure. Indeed, except as noted below, there are no significant differences observed in the features of any of the various valence spectra recorded in this study. There is, however, no clear indication of vibrational structure in any of the bands. (This contrasts with the C_2 1s ionization below, where there is a clear vibrational excitation—vide infra.)

The calculated first and second ionization energies for the various conformers again each cluster together and hence correlate readily with the first two experimental bands while making no distinction between the conformers. In our high-photon-energy spectra, the first 10.33-eV peak is notably more pronounced than in the earlier He I spectrum,[15] as can be seen in Figures 2 and 3. This observation helps corroborate the existing assignment of the first band as having O 2p lone-pair character because those orbitals with significant atomic O character are empirically expected to show such a relative enhancement with increasing photon energy.[41] In our calculated HF molecular orbitals (Figure 4), a mixing of the O lone pair with adjacent C σ bonds is seen in the HOMO (orbital 21), but as the orientation rotates with the OH dihedral angle ϕ, so the degree and nature of the interaction change. When the various conformers are considered, this leads to a small dispersion in the calculated IE of this nominally localized nonbonding electron, which should therefore contribute to the observed 0.5-eV width of the band.

Between 12 and 16 eV, there seems to be a more uniform distribution of the various OVGF energies obtained for the -gg and -ag conformers, but as these together are expected to account for only ∼33% of the population (Table 1), they may be assumed to contribute to a general featureless background level across this subregion. Attention will henceforth be focused on the three most populous -ga conformations (together, approximately 67%). Although it can be seen in the figures that all but one of the identified features in our spectra (at ∼16.7 eV) can be correlated rather well with calculated ionization energies of one or more of the -ga conformers, the more complex correlation between theory and experiment in this region makes some distinctions between individual conformations possible.

The prominent bands seen at ∼12.7 and ∼17.3 eV and the distinct shoulder at ∼13.5 eV all correspond very closely to calculated ionization energies of the m-ga and e-ga conformers but not to any of the h-ga conformers. Nor indeed is the correlation between the first two of these experimental peaks and the calculated IEs for any of the other six conformations so striking. This can be taken to be a positive identification of at least one of the m-ga and e-ga conformers under the conditions of our experiment (and in the earlier He I experiments.[15]). However, the h-ga conformer is the only one of the nine with calculated IEs that closely correspond to the equally prominent experimental feature at ∼16.1 eV. This then may be considered to be a reasonably positive identification of the h-ga conformer.

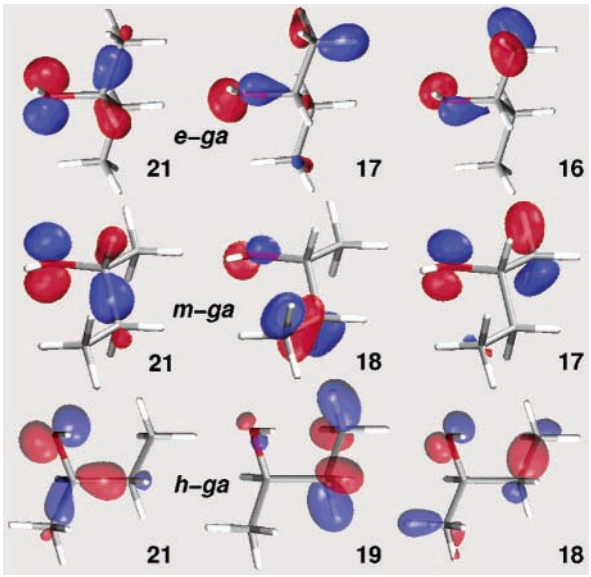

Figure 4. HF/cc-pVDZ orbitals for the lowest-energy m-ga, e-ga, and h-ga conformers. The HOMO (orbital 21) of each together with other selected examples discussed in the text is shown. The molecules are drawn oriented with the hydroxyl group to the left, with the C−O bond approximately in the plane of the paper and the O−H directed upward out of the paper.

The other very prominent experimental feature at ∼12.2 eV could, a priori, be equally well correlated with one or both of the e-ga or h-ga calculated energies or perhaps rather less likely with the m-ga conformer. What is interesting about this ∼12.2 eV feature and the adjacent ∼12.7 eV peak is their markedly more peaked appearance in the linearly polarized spectra recorded in configuration **II** as compared to that in the circularly polarized spectra recorded in configuration **I** (see Figure 3). The slightly lower photon energies in the latter case are unlikely to be greatly significant in this regard (although reduced photon energy may play some role in the same qualitative difference observed in the He I spectrum), and both configurations employ the magic angle to obviate angular distribution effects. Thus, the most likely explanation for these "spikes" is associated with the increased resolution of the measurements made in the former configuration. If so, this would suggest a peak width commensurate with the improved resolution (60 meV). Being so narrow, this in turn suggests the ionization to be of a nonbonding electron with a consequent narrow Franck−Condon envelope expected for the band.

If we then examine the three orbitals (m-ga 18 and 17 and e-ga 17) whose ionization energies are well correlated with the most sharply peaked ∼12.7-eV feature, then it can be seen (Figure 4) that m-ga 17 has a pronounced O lone pair mixed with just a single C−H bond (cf. the lone-pair HOMO orbitals 21 in the same Figure). The other adjacent m-ga orbital 18 also has some O 2p character, although now rotated into the C−O−H plane and mixed with more extensive H−C−C bonding character, whereas the e-ga orbital 17 displays more C−O bonding character. We thus infer that the extra spikiness of the ∼12.7-eV peak seen at high resolution and high photon energy could well be most directly attributable to a contribution from the ionization of the m-ga 17 orbital, thus helping confirm the presence of the m-ga conformer.

By similarly examining those orbitals of the -ga conformers that correlate to the ∼12.2-eV peak, we conclude that the contribution made by the ionization of h-ga 18 is the most likely explanation for the enhanced spike here, as it shares comparable lone-pair character with HOMO orbital 21 of this conformer (Figure 4). The adjacent orbital, h-ga 19, despite an almost identical predicted ionization energy, has much more bonding character, as do those energetically close orbitals of the m-ga and e-ga conformers.

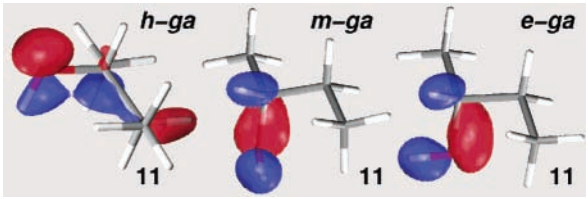

Figure 5. HF/cc-pVDZ orbital 11 for the m-, e-, and h-ga conformers. The molecules are drawn oriented with the hydroxyl group to the left.

It was previously suggested in a wider-ranging comparative study of the higher alcohols that an ∼17.2-eV band, as seen here, may be a general characteristic of the photoelectron spectra of primary or secondary alcohols.[15] It is then interesting to see the marked similarity of the two orbitals assigned to this band in the present study—m-ga and e-ga orbitals 11 displayed in Figure 5. These are both H−C−O−H σ-bonding orbitals with a similar configuration in that the two H atoms lie gauche to one another (see Figure 1). It is also easy to see why the highly localized character could be a characteristic of primary or secondary alcohols but not tertiary alcohols, where the hydrogen at the carbanol carbon is substituted by another side group. Rotation about the C−O bond to the h conformation, placing the two H atoms anti to one another, destroys this character (Figure 5). There is thus a pronounced splitting of the 11th-orbital bands between the h-ga conformer and the m-ga, e-ga conformer pair.

In addition to those correlations between theory and experiment discussed above, a number of other possible correlations are drawn in Figure 3. There are, however, a number of calculated IEs in the 14.0−15.5-eV range that do not correlate with significant peaks, although there is a broad experimental band in this region. The associated orbitals are quite significantly delocalized around the carbon skeleton compared to those highlighted above and have reduced O-atom character. It is conceivable that these are relatively weak ionizations at higher photon energies—certainly the ionization cross section in this region appears relatively stronger in the He I spectrum—and presumably also give rise to ionization with broad Franck−Condon envelopes and so with few discernible features.

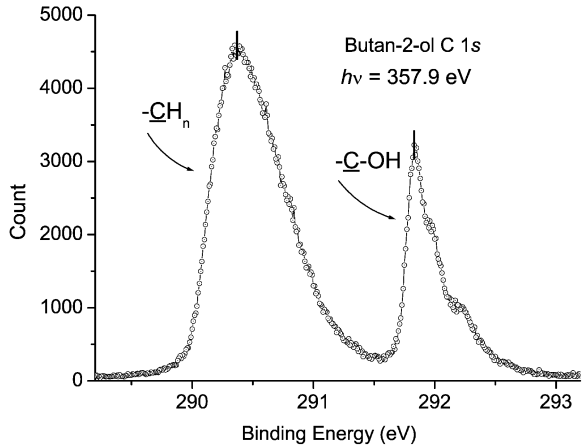

Figure 6. C 1s photoelectron spectrum of butan-2-ol.

TABLE 4: HF/cc-pVDZ Core Orbital Eigenvalues (in eV) for Butan-2-ol Conformers[a]

	O 1s	C_2 (−OH) 1s	C_1, C_3 1s		C_4 1s
e-ag	−559.2	−307.0	−305.4	−305.4	−305.4
e-ga	−559.2	−307.0	−305.4	−305.4	−305.1
e-gg	−559.2	−307.0	−305.4	−305.4	−305.1
h-ag	−559.2	−307.0	−305.5	−305.5	−305.4
h-ga	−559.2	−307.0	−305.5	−305.4	−305.3
h-gg	−559.2	−307.0	−305.5	−305.5	−305.4
m-ag	−559.2	−307.0	−305.6	−305.5	−305.2
m-ga	−559.2	−307.0	−305.6	−305.5	−305.2
m-gg	−559.2	−307.0	−305.6	−305.3	−305.2
mean value (HF orbitals)	−559.2	−307.0		−305.4	
mean value[b] (DFT orbitals)	−520.7	−278.4		−276.9	
experimental peak positions	538.6[c]	291.83		290.37	

[a] Mean values for the O, C(−OH), and alkyl C 1s orbitals averaged over all conformers are also shown. [b] B3LYP/6-31G** Kohn−Sham orbital eigenvalues. [c] Reference 17.

Conversely, all of the significant features in the experimental spectrum can be reasonably assigned to the ionization of one or more of the -ga conformers with the single exception of the small yet highly reproducible feature at ∼16.7 eV, whose origin remains unexplained.

4.2. Core-Level Spectra. The C 1s spectrum is shown in Figure 6 and is relatively simple in form. Consequently, only a restricted analysis of the core-level ionization energies has been undertaken using orbital energies already established in the preceding valence-shell calculations. The Hartree−Fock/cc-pVDZ 1s eigenvalues are presented in Table 4. Not surprisingly, the localized core orbital energies vary little with changing molecular conformation. Mean values, averaged over the nine conformations, are obtained for the oxygen 1s, carbanol carbon 1s, and the three, nearly identical other carbon 1s levels. Trivially, these can provide Koopman's theorem estimates of the IE, but since relaxation energies are ignored, one may expect such results to *overestimate* the binding energy. Analogous mean eigenvalues for the B3LYP/6-31G** core orbitals are also included in Table 4 for comparison. Koopman's theorem does not apply to such Kohn−Sham orbitals calculated with present functionals such as B3LYP. However, studies suggest that *relative* ionization energies may be meaningfully estimated from these DFT results[42] and that the eigenvalues may be related to the Koopman's theorem limit by a simple linear correlation.[43] More particularly, these studies find that the Kohn−Sham orbitals are generally shifted to higher (less negative) energy than their HF counterparts; consequently, negating the eigenvalues is more likely to *underestimate* the binding energy. Overall, these two alternative sets of averaged eigenvalues are expected to help bracket the experimental ionization energies and to indicate the expected shifts.

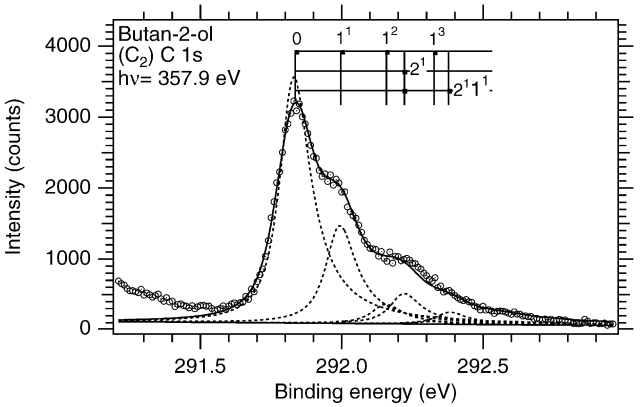

Figure 7. C 1s photoelectron spectrum of the C_2 carbon of butan-2-ol fitted with a model containing two vibrational progressions. The dashed curves represent the individual vibrational states, and the full curve through the data points represents the final fit after summation and convolution with instrumental profiles.

These expectations are borne out. Although not a part of our experimental study, the O 1s binding energy cited in the literature,[17] 538.6 eV, is indeed intermediate between the negated HF and DFT eigenvalues in Table 4. Likewise, our C 1s spectrum of ∼290 eV is bracketed by the HF and DFT C 1s energies in the Table. Of equal importance are the relative energies of the four carbon atoms, with the C_2−OH carbon being split by ∼1.5 eV from the approximately coincident binding energies of the other three. This quantitatively confirms a qualitative expectation of a chemical shift for the C_2 1s level attributable to the inductive effect of the OH group. We thus readily assign the principal experimental peak at 290.37 eV to an unresolved overlapping ionization of the alkyl C 1s orbitals in the various molecular conformations present and the smaller 291.83-eV peak to the hydroxyl C_2 1s ionization, the splitting being exactly as predicted from Table 4.

Clear vibrational structure can be seen on the side of the carbanol (C_2) peak. This structure was analyzed with a least-squares fit that assumed two vibrational progressions (see section 2 for details). Although it was not possible to obtain a satisfactory fit using only one vibrational progression, it is quite possible that, whereas two vibrational progressions provide a satisfactory fit to the data, more than two modes may actually be excited to a significant degree. The fit was restricted to the binding-energy region above 291.3 eV to ensure that only the C_2 carbon peak was analyzed. The least-squares fit shown in Figure 7 yielded vibrational energies of 163(10) meV for the low-frequency vibration (ν_1) and 390(10) meV for the high-frequency vibration (ν_2). The latter ν_2 value ($\equiv$ 3146 cm^{-1}) is typical for the C−H stretch in C 1s ionization, whereas the former ν_1 value ($\equiv$ 1315 cm^{-1}) may be tentatively identified as a bending motion at the same localized C_2 site. Wang and Polavarapou[14] list several vibrational frequencies of this magnitude, measured in solution, including a number of COH bending modes whose frequencies range from 153 to 170 meV in the ground-state molecule.

5. Conclusions

The data presented here, together with an earlier measurement of the O 1s binding energy,[17] mean that the ionization of every

orbital in butan-2-ol has been mapped out. The localized core orbitals are not sensitive to molecular conformation, and a relatively simple C 1s spectrum results, with the carbon attached to the hydroxyl group being clearly resolved. However, the valence spectrum consists of many bands, some of which are partially overlapped. The calculated valence ionization energies are sensitive to the conformation assumed, at least in the region from 12−18 eV, so this potentially provides an opportunity to glean something about the conformers present, even though this technique would hardly be the method of choice for structural determination!

In fact, the predicted band positions of six out of the nine conformers identified are too congested and too weak (these six account for only one-third of the predicted room-temperature population) for any information to be deduced. The remaining three, more populous -ga conformers clearly do account together for much of the observed structure in the spectrum, with a strong correlation between the experimental features and the calculated IE values being achieved. In this sense, a useful simplification is obtained in that the experimental photoelectron spectrum can be successfully discussed in terms of only a limited number of the nine possible molecular conformers.

The peaks observed at ∼12.7 and ∼17.2 eV correlate well to predicted ionizations of the e-ga, m-ga pair, not at all with ionization of the h-ga conformer, and only poorly, if at all, with any other conformers. This gives a strong indication of the presence of at least one member of this pair. It is scarcely possible to distinguish the two, although a consideration of orbital characters suggests that it is the m-ga conformer that is responsible for the strong peaking of the ∼12.7-eV peak, thus making identification of the m-ga conformer rather more positive (while in no way ruling out the contribution of the e-ga conformer). However, there is a clear band seen at ∼16.1 eV that can be correlated only with the ionization of the h-ga conformer. So we have positive identifications of the h-ga, m-ga, and probably also e-ga conformers, as would be expected from a Boltzmann population.

Clearly, this analysis of the relative importance of alternative conformations in our thermal sample is not, nor would it be expected to be, definitive. A recent microwave study by King and Howard[13] was able to produce much more definitive evidence for the presence of single representative structures of each of the -ag, -gg, and -ga conformations, but they further concluded that the h-ga conformer was *not* one of those present under their conditions despite HF—and now DFT—calculations placing it as one of the two most stable conformations. Possibly the discrepancy with our results may be related to the lack of a true thermal equilibrium in their molecular beam with the possibility of relaxation effects in the beam expansion leading to a biasing of the population. Further examination of the barriers to interconversion of these three conformers and hence of possible dynamic effects under specified sample conditions would be welcome.

Acknowledgment. We thank the staff at BESSY for their assistance in operating the beamline. Computational resources on a COMPAQ ES40 multiprocessor cluster (Columbus) at the Rutherford Appleton Laboratory (RAL) provided by the U.K. Computational Chemistry Facility are acknowledged. T.M.W. thanks the Nuffield Foundation for support in the form of an Undergraduate Research Bursary (URB/00224/G).

References and Notes

(1) Bailey, J. *Origins Life Evol. Biosphere* **2001**, *31*, 167−183.

(2) Bailey, J.; Chrysostomou, A.; Hough, J. H.; Gledhill, T. M.; McCall, A.; Clark, S.; Menard, F.; Tamura, M. *Science (Washington, D.C.)* **1998**, *281*, 672−674.

(3) Greenberg, J. M.; Kouchi, A.; Niessen, W.; Irth, H.; Vanparadijs, J.; Degroot, M.; Hermsen, W. *J. Biol. Phys.* **1994**, *20*, 61−70.

(4) Bonner, W. A. *Origins Life Evol. Biosphere* **1991**, *21*, 59−111.

(5) Bonner, W. A.; Greenberg, J. M.; Rubenstein, E. *Origins Life Evol. Biosphere* **1999**, *29*, 215−219.

(6) Piccirillo, S.; Bosman, C.; Toja, D.; Giardini-Guidoni, A.; Pierini, M.; Troiani, A.; Speranza, M. *Angew. Chem., Int. Ed. Engl.* **1997**, *36*, 1729−1731.

(7) Latini, A.; Toja, D.; Giardini-Guidoni, A.; Palleschi, A.; Piccirillo, S.; Speranza, M. *Chirality* **1999**, *11*, 376−380.

(8) Al Rabaa, A.; Le Barbu, K.; Lahmani, F.; Zehnacker-Rentien, A. *J. Phys. Chem. A* **1997**, *101*, 3273−3278.

(9) Le Barbu, K.; Brenner, V.; Millie, P.; Lahmani, F.; Zehnacker-Rentien, A. *J. Phys. Chem. A* **1998**, *102*, 128−137.

(10) Borho, N.; Haber, T.; Suhm, M. A. *Phys. Chem. Chem. Phys.* **2001**, *3*, 1945−1948.

(11) King, A. K.; Howard, B. J. *Chem. Phys. Lett.* **2001**, *348*, 343−349.

(12) Hagemann, H.; Mareda, J.; Chiancone, C.; Bill, H. *J. Mol. Struct.* **1997**, *410*, 357−360.

(13) King, A. K.; Howard, B. J. *J. Mol. Spectrosc.* **2001**, *205*, 38−42.

(14) Wang, F.; Polavarapu, P. L. *J. Phys. Chem. A* **2000**, *104*, 10683−10687.

(15) Peel, J. B.; Willett, G. D. *Aust. J. Chem.* **1975**, *28*, 2357−2364.

(16) Ogata, H.; Onizuka, H.; Nihei, Y.; Kamada, H. *Bull. Chem. Soc. Jpn.* **1973**, *46*, 3036−3040.

(17) Benoit, F. M.; Harrison, A. G. *J. Am. Chem. Soc.* **1977**, *90*, 3980.

(18) Shao, J. D.; Baer, T.; Lewis, D. K. *J. Phys. Chem.* **1988**, *92*, 5123−5128.

(19) Powis, I. *J. Chem. Phys.* **2000**, *112*, 301−310.

(20) Powis, I. *J. Phys. Chem. A* **2000**, *104*, 878−882.

(21) Böwering, N.; Lischke, T.; Schmidtke, B.; Müller, N.; Khalil, T.; Heinzmann, U. *Phys. Rev. Lett.* **2001**, *86*, 1187−1190.

(22) Csaszar, A. G. *J. Phys. Chem.* **1996**, *100*, 3541−3551.

(23) Kaschner, R.; Hohl, D. *J. Phys. Chem. A* **1998**, *102*, 5111−5116.

(24) Klasinc, L. *J. Electron Spectrosc. Relat. Phenom.* **1976**, *8*, 161−164.

(25) Godfrey, P. D.; Firth, S.; Hatherley, L. D.; Brown, R. D.; Pierlot, A. P. *J. Am. Chem. Soc.* **1993**, *115*, 9687−9691.

(26) Iijima, K.; Beagley, B. *J. Mol. Struct.* **1991**, *248*, 133−142.

(27) Weiss, M. R.; Follath, R.; Sawhney, K. J. S.; Senf, F.; Bahrdt, J.; Frentrup, W.; Gaupp, A.; Sasaki, S.; Scheer, M.; Mertins, H. C.; Abramsohn, D.; Schäfers, F.; Kuch, W.; Mahler, W. *Nucl. Instrum. Methods Phys. Res., Sect. A* **2001**, *467*, 449−452.

(28) Mårtensson, N.; Baltzer, P.; Brühwiler, P. A.; Forsell, J.-O.; Nilsson, A.; Stenborg, A.; Wannberg, B. *J. Electron Spectrosc. Relat. Phenom.* **1994**, *70*, 117−128.

(29) Kikas, A.; Osborne, S. J.; Ausmees, A.; Svensson, S.; Sairanen, O. P.; Aksela, S. *J. Electron Spectrosc. Relat. Phenom.* **1996**, *77*, 241−266.

(30) Lias, S. G. In *NIST Chemistry WebBook.* NIST Standard Reference Database, 69th ed.; Linstrom, P. J., Mallard, W. G., Eds.; National Institute of Standards and Technology: Gaithersburg MD, 2001; http://webbook.nist.gov.

(31) Whitfield, S. B.; Langer, B.; Viefhaus, J.; Wehlitz, R.; Berrah, N.; Mahler, W.; Becker, U. *J. Phys. B: At. Mol. Opt. Phys.* **1994**, *27*, L359−L366.

(32) Aksela, H.; Aksela, S.; Pulkkinen, H. *Phys. Rev. A: At., Mol., Opt. Phys.* **1984**, *30*, 865−871.

(33) Armen, G. B.; Tulkki, J.; Aberg, T.; Crasemann, B. *Phys. Rev. A: At., Mol., Opt. Phys.* **1987**, *36*, 5606−5614.

(34) Becke, A. D. *J. Chem. Phys.* **1993**, *98*, 5648−5652.

(35) Lee, C. T.; Yang, W. T.; Parr, R. G. *Phys. Rev. B* **1988**, *37*, 785−789.

(36) Abe, K.; Ito, K.; Suezawa, H.; Hirota, M.; Nishio, M. *Bull. Chem. Soc. Jpn.* **1986**, *59*, 3125−3130.

(37) von Niessen, W.; Schirmer, J.; Cederbaum, L. S. *Comput. Phys. Rep.* **1984**, *1*, 57−125.

(38) Zakrzewski, V. G.; Dolgounitcheva, O.; Ortiz, J. V. *J. Chem. Phys.* **1996**, *105*, 8748−8753.

(39) Schirmer, J.; Domcke, W.; Cederbaum, L. S.; von Niessen, W. *J. Phys. B: At. Mol. Opt. Phys.* **1978**, *11*, 1901−1915.

(40) Powis, I.; Rennie, E. E.; Hergenhahn, U.; Kugeler, O.; Bussy-Socrate, R. *J. Phys. Chem. A*, in press.

(41) Schweig, A.; Thiel, W. *Mol. Phys.* **1974**, *27*, 265.

(42) Politzer, P.; Abu-Awwad, F.; Murray, J. S. *Int. J. Quantum Chem.* **1998**, *69*, 607−613.

(43) Stowasser, R.; Hoffmann, R. *J. Am. Chem. Soc.* **1999**, *121*, 3414−3420.